Spacer Length Controlled Oblique-Columnar to Lamello-Columnar Mesophase Transition in Liquid Crystalline DNA−Discotic Cationic Lipid Complexes

Li Cui, Jianjun Miao, and Lei Zhu*

Polymer Program, Institute of Materials Science and Department of Chemical Engineering, The University of Connecticut, Storrs, Connecticut 06269-3136

Received January 1, 2006; Revised Manuscript Received February 9, 2006

ABSTRACT: Asymmetric triphenylene imidazolium salts with spacer lengths of C_5, C_8, and C_{11} were successfully synthesized. DNA complexation with these cationic discotic lipids was achieved by mixing DNA and triphenylene imidazolium salts in aqueous solutions. The molecular composition of the complexes in the bulk was quantitatively determined using Fourier transform infrared (FTIR) spectroscopy; the ratio of negative phosphate groups to positive imidazolium salt ranged from 1.4 to 2.0 for different discotic cationic lipids. The columnar liquid crystalline morphology was characterized by polarized light microscopy, X-ray diffraction (XRD), and transmission electron microscopy. When the spacer length of the triphenylene imidazolium salts increased from C_5 to C_8 and C_{11}, a morphological transition from an oblique-columnar (Col_o) phase to lamello-columnar (Col_L) phases was observed. From detailed XRD results, the face-to-face interdisk spacing in a triphenylene column (0.35 nm) was similar to the period of hydrogen-bonded pairs in DNA (0.34 nm), suggesting a 1:1 complexation between the phosphate group and the imidazolium salt. The higher phosphate/imidazolium salt ratio (1.4−2.0) determined by FTIR suggested that the DNA chains were partially complexed due to rapid precipitation of the complexes upon mixing the two components in aqueous solutions. The columnar stacking of the triphenylene discotic molecules destroyed the helical conformation in the double-strand DNA, as evidenced by a circular dichroism study. When the semirigid DNA molecules were replaced with flexible total RNA, columnar liquid crystalline self-assembly of the triphenylene molecules in the complexes disappeared, and only a lamellar morphology with random discotic triphenylenes sandwiched between neighboring RNA layers was observed.

Introduction

Polyelectrolytes can interact strongly with oppositely charged surfactants, self-assembling into highly ordered complexes at nanoscopic scales. These polyelectrolyte−surfactant complexes have attracted much attention not only due to their applications in biological systems but also because of their importance in polymer science and biophysics.[1−3] Through manipulation of the electrostatic interactions (e.g., charge density), the rigidity and hydrophobicity of the polyelectrolyte chains, and the shape and balance between the amphiphilic moieties in surfactants, novel supramolecular structures in the polyelectrolyte−surfactant complexes can be designed, leading to unique mechanical, electrical, optical, and biological properties for specific applications.[4−6]

As a negatively charged polyelectrolyte with a characteristic double-strand helical conformation, DNA has received much attention, and its complexation (or condensation) with a variety of cationic species has a great impact in science and technology.[7,8] For example, DNA complexation in chromosomes represents an important process that nature uses to pack genetic information in an efficient and safe way.[9] As a powerful protocol for gene therapy and vaccination in biotechnology and medical applications, DNA complexation with cationic lipids provides promising nonviral delivery systems.[10,11] Furthermore, DNA condensation is also reminiscent of the coil-to-globule transition in synthetic polymers, exhibiting intriguing liquid crystalline and polyelectrolyte behaviors in particular. The fundamental driving force for DNA complexation with cationic species is twofold; the entropic gain in free energy through the release of small molecule counterions could possibly be comparable to that from direct electrostatic interactions between DNA and cationic species.[12−14]

A variety of basic proteins can complex with DNA to form ordered condensates. As mentioned above, the well-known example is the DNA complexation with positively charged histone proteins in eukaryotic cell nuclei to form chromatin, which is used to store genetic information.[9,15,16] There are hierarchically self-assembled structures in the chromatin on various length scales. First, DNA complexes with cationic histones to form a "beads-on-a-string" (or nucleofilament) structure with the DNA chains wrapping 1.75 times around the short cylinder of a histone (diameter of 6.5 nm and length of ∼10 nm).[9] Second, the nucleofilament further folds into either solenoid or irregular zigzag of 30 nm fibers. Finally, further sequential folding of these fibers leads to a high level of organization to form the chromosome structures.

Since viral gene delivery has potential risks of induced immunological problems and limited carrying capacity,[17] nonviral gene delivery systems[18] have been actively pursued to avoid the disadvantages of viral gene delivery since the pioneer work by Felgner et al.[19] These systems utilize DNA condensation with cationic lipids and polymers under a micellar or liposomal form, which are also termed as lipoplexes and polyplexes. Cationic lipids for DNA condensation usually contain hydrophobic tails and hydrophilic quaternary ammonium heads. Examples include dioleoyltrimethylammonium propane (DOTAP),[20] dimyristoyltrimethylammonium propane (DMTAP),[21,22] dioctadecyldiammonium bromide (DODAB),[23−25] 1,2-dipalmitoyl-*sn*-glycero-3-ethylphosphocholine (EDPPC),[26,27] 1,2-dioleoyl-*sn*-3-ethylphosphocholine (EDOPC),[28,29] bisguanidinium tren cholesterol (BGTC),[30] and many others.[31,32] In the DNA−lipid complexes, helper (neutral) lipids such as zwitter-

* Corresponding author: e-mail lei.zhu@uconn.edu; Tel 860-486-8708.

10.1021/ma060001x CCC: $33.50
Published on Web 03/10/2006

ionic lipids, dioleoylphosphatidylcholine (DOPC), dimyristoylphosphatidylcholine (DMPC), and dioleoylphosphatidylethanolamine (DOPE) are used to manipulate the morphology of ordered structures, and they were shown to affect gene transfection efficiency.[33] Small-angle X-ray scattering (SAXS) revealed that the DNA lipoplexes showed highly ordered liquid crystalline phases at the nanometer scales. Lamello-columnar (L_α^C with DNA being the columns) phases were commonly observed with a separate *d*-spacing attributed to the in-plane organization of parallel aligned DNA molecules sandwiched by lipid layers.[20−33] The equilibrium lamellar spacing (*d*) and inter-DNA spacing (d_{DNA}) in a two-dimensional (2D) plane were considered to be results of the long-range electrostatic repulsion interactions among DNA and bilayers and were thus closely dependent on the charge density.[14] The charge density was inversely proportional to the ratio of neutral to cationic lipid. As it decreased (or the concentration of neutral lipid increased) at the isoelectric point, the overall lamellar spacing slightly changed from 5.6 to 6.9 nm, while d_{DNA} varied significantly from 2.45 to 5.71 nm.[20] Overcharging, which was also controlled by the charge density, could happen when excess cationic lipid or DNA was absorbed into the self-assembled structure. Generally, positive overcharging induced lower DNA packing density while negative overcharging produced a higher packing density.

The above experimental observations have stimulated a series of theoretical research to elucidate the thermodynamics of DNA lipoplexes. A supramolecular model, namely, a "sliding columnar phase", was proposed to have little positional correlations between unidirectionally oriented DNA molecules in neighboring lamellae.[34−37] Studies on DNA−DNA interactions within one layer and between neighboring layers suggested the existence of the long-range repulsive electrostatic interactions.[12,13]

Inverted hexagonal (H_{II}^C) phases were observed for DNA lipoplexes which contained a high concentration of DOPE, a hexagonal forming lipid.[24,38] In these H_{II}^C phases, cationic and neutral lipids formed a monolayer around double-strand DNA helices. For low DOPE content lipoplexes, conventional L_α^C phases occurred. It was considered that the interplay between the electrostatic and bilayer elastic interactions in the DNA lipoplexes dictated the stability and transition between L_α^C and H_{II}^C phases. Sometimes L_α^C and H_{II}^C phases even coexisted in a system.[39]

Although SAXS is powerful in revealing the global morphology of DNA lipoplexes, information on local organizations and intermediate stages during lipoplex formation can only be obtained by transmission electron microscopy (TEM). For example, using a negative staining technique, a TEM study on DNA complexation with spherical liposomes (ca. 20 nm) suggested that cationic liposomes formed clusters around the DNA molecules, followed by subsequent cluster coalescence to form DNA−lipid alternating lamellar membranes.[40] On the other hand, cryo-TEM studies observed an opposite trend. Instead of liposome condensing onto DNA molecules, DNA molecules wrapped around cationic liposomes (50−100 nm), and subsequent layer-by-layer condensation and collapse of the nanoparticles induced lamellar membranes.[41,42] Although the formation mechanism of DNA lipoplex was not yet clarified, numerous cryo-TEM studied revealed that multiple lamellae were present in spherical lipoplex nanoparticles ranging from 50 nm to a couple hundred nanometers.[23,24,30,43] The size and dispersion of colloidal DNA lipoplexes were important parameters which determined the transfection efficiency.

Other than cationic lipids, cationic dendrimers and polymers have also been used to complex with DNA, forming ordered mesoscopic structures. In the DNA complexes with dendritic poly(propyleneimine) (PPI, generation 4 and 5), ordered square and hexagonal columnar assemblies of DNA around PPI dendrimers were observed.[44] A structural transition between square and hexagonal geometries simply depended on the negative-to-positive charge ratio and NaCl concentration in aqueous solution. Shape-persistent dendron-side-group polymers with quaternized amines at the periphery were used to complex with DNA in aqueous solutions, and the complexes were studied by atomic force microscopy (AFM) on mica substrates.[45,46] Parts of DNA chains wrapped around dendronized polymers with an average helical pitch of ca. 2.2 nm for different dendron generations.

Although much work has been dedicated to revealing supramolecular structures in DNA−cationic lipid complexes, which is primarily stimulated by nonviral gene delivery, few efforts have focused on using DNA−cationic surfactant complexes as advanced materials for organic electronic and optical applications.[31,32] Furthermore, no research has been performed on DNA complexes with discotic cationic surfactants, which have specific electronic and optical properties for potential applications such as one-dimensional semiconductors, nonlinear optics, field-effect transistors, photovoltaics, and so on. In this work, we report, for the first time, the nanoscopic supramolecular self-assembly of DNA−discotic cationic lipid complexes in the solid state, and expect that they could be used as advanced polymeric materials in the future. Asymmetric discotic cationic lipids containing a hydrophobic triphenylene "tail" and a hydrophilic imidazolium salt head have been synthesized. The spacer length between the triphenylene tail and imidazolium head varied from C_5 to C_8 and C_{11}. Double-strand DNA complexes with the triphenylene imidazolium salts were obtained by mixing the corresponding components in aqueous solutions. The molecular composition of the DNA−triphenylene imidazolium salt complexes was quantitatively determined by Fourier transform infrared (FTIR) spectroscopy. Columnar liquid crystalline phases in the DNA−triphenylene imidazolium salt complexes were determined by 2D X-ray diffraction (XRD). Intriguingly, a morphological transition was observed from an oblique columnar (Col_o) phase for a spacer length of C_5 to novel double lamello-columnar (Col_L) phases (both DNA and triphenylenes being columns) for spacer lengths being C_8 and C_{11}. Regular helical conformation in DNA complexes was lost as studied by circular dichroism. Comparing to the single-strand total RNA complexes with triphenylene imidazolium salts, the chain rigidity in DNA molecules seemed to be responsible for the columnar mesophase formation in triphenylene molecules.

Experimental Section

Materials. 1-Methylimidazole was purchased from Aldrich and distilled under reduced pressure before use. Fish sperm double-strand DNA (Na form) was purchased from USB Corp. (Cleveland, OH)[47] and was purified by dialysis followed by filtration through a 0.20 μm PTFE filter. Baker's yeast total RNA was purchased from Sigma-Aldrich[48] and was used without further purification. 11-Bromoundecanoyl chloride, 8-bromooctanoyl chloride, and 5-bromovaleryl chloride were prepared by treatment of corresponding acids with thionyl chloride and purified by reduced pressure distillation. 1,2-Bis(pentyloxy)benzene was prepared according to the literature.[49] 2,3,6,7,10,11-Hexakis(pentyloxy)triphenylene was prepared by trimerization of 1,2-bis(pentyloxy)benzene using ferric chloride as an oxidative agent.[50] 2-Hydroxy-3,6,7,10,11-pentakis-(pentyloxy)triphenylene (H5TP-OH) was prepared by cleavage of 2,3,6,7,10,11-hexakis(pentyloxy)triphenylene with 1.2 equiv of B-bromocatecholborane.[51] Other commercially available chemicals were used without further purification.

Scheme 1. Synthesis of Triphenylene Imidazolium Salts with Various Spacer Lengths and Their Complexes with DNA

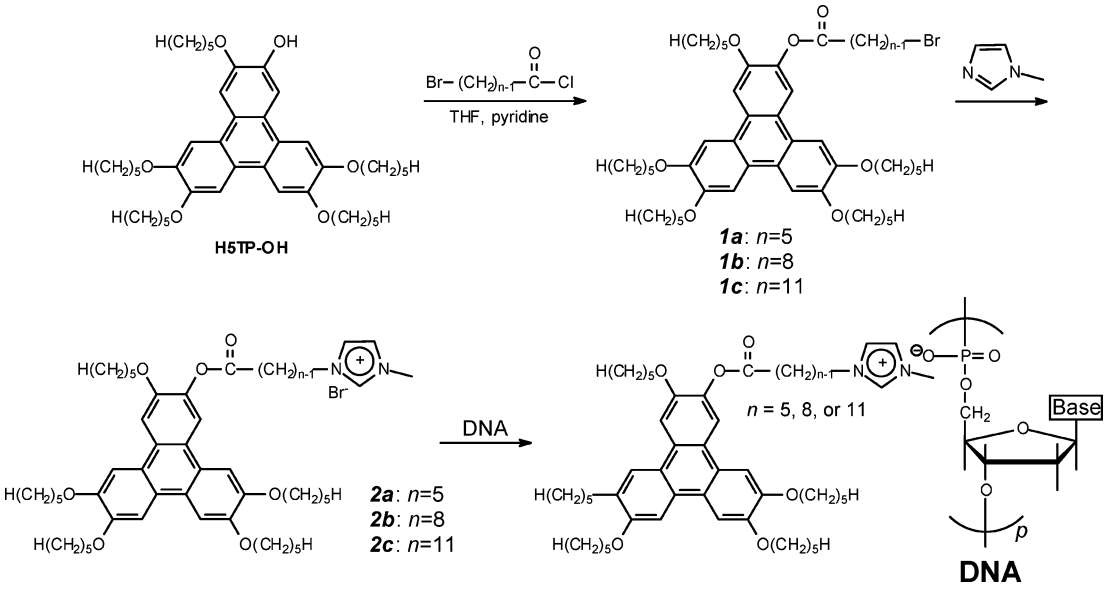

Synthesis of Triphenylene Imidazolium Salts with Different Spacer Lengths. Asymmetric bromo-terminated triphenylenes with spacer lengths of C_5, C_8, and C_{11} were synthesized via esterification of bromo-terminated alkanoyl chloride and H5TP-OH. Subsequently, quaternization of bromo-terminated triphenylenes with 1-methylimidazole afforded asymmetric triphenylene imidazolium salts, as shown in Scheme 1. Detailed procedures are described below.

Preparation of 2-(11-Bromoundecanoyloxy)-3,6,7,10,11-pentakis(pentyloxy)triphenylene (1c). 202.5 mg (0.3 mmol) of H5TP-OH and 79.5 mg (1 mmol) of pyridine were dissolved in 5 mL of dry THF. 187.2 mg (0.66 mmol) of 11-bromoundecanoyl chloride was added dropwise at room temperature under stirring. The temperature was raised to 60 °C and stirred for 4 h. The mixture was poured into 20 mL of water and extracted with CH_2Cl_2. The solvent was then evaporated, and crude product was purified by passing through a silica gel column with a mixture of acetone: hexane = 1:5. The product was dried under vacuum, and ca. 178 mg of brown oil was obtained with a yield of 64%. ^{1}H NMR (δ, $CDCl_3$): 0.99 (t, CH_3, 15H) 1.35−1.57 [m, $CH_3CH_2CH_2$ and $(CH_2)_6CH_2CH_2Br$, 32H], 1.88 (m, CH_2CH_2COO, 2H), 1.97 (m, CH_2CH_2Br and CH_2CH_2O, 4H), 2.69 (t, CH_2COO, 2H), 3.43 (t, CH_2Br, 2H), 4.25 (t, CH_2O, 10H), 7.7−8.1 (m, Ar−H, 6H).

1a and **1b** were prepared similarly. The purity of **1a**−**c** was confirmed by thin-layer chromatography (TLC) and size-exclusion chromatography (SEC). **1a** was obtained as pale white powder with a yield of 77%. ^{1}H NMR (δ, $CDCl_3$): 0.98 (t, CH_3, 15H) 1.44−1.56 (m, $CH_3CH_2CH_2$, 20H), 1.62−1.97 (m, CH_2CH_2O, CH_2CH_2COO, CH_2CH_2Br, 14H), 2.74 (t, CH_2COO, 2H), 3.51 (t, CH_2Br, 2H), 4.24 (t, CH_2O, 10H), 7.7−8.1 (m, Ar−H, 6H). **1b** was obtained as brown waxlike solid with a yield 70%. ^{1}H NMR (δ, $CDCl_3$): 0.99 (t, CH_3, 15H) 1.34−1.59 (m, $CH_3CH_2CH_2$ and $(CH_2)_3CH_2CH_2Br$, 26H), 1.87 (m, CH_2CH_2COO, 2H), 1.96 (m, CH_2CH_2Br and CH_2CH_2O, 4H), 2.69 (t, CH_2COO, 2H), 3.47 (t, CH_2Br, 2H), 4.25 (t, CH_2O, 10H), 7.7−8.1 (m, Ar−H, 6H).

Preparation of Triphenylene Imidazolium Salts. Triphenylene imidazolium salt **2c** was prepared as follows: 170 mg of 2-(11-bromoundecanoyloxy)-3,6,7,10,11-pentakis(pentyloxy)triphenylene and 150 mg of 1-methylimidazole were mixed together and heated to 70 °C under a nitrogen atmosphere overnight. Brown oil was obtained and washed with hexane to remove the unreacted 1-methylimidazole. The product was further purified by column chromatography using alumina and acetone and methanol as eluents, respectively. 120 mg of a yellow and soft solid was obtained with a yield 65%. ^{1}H NMR (δ, $CDCl_3$): 0.99 (t, CH_3, 15H) 1.35−1.57 [m, $CH_3CH_2CH_2$ and $(CH_2)_6CH_2CH_2Br$, 32H], 1.88 (m, CH_2CH_2COO, 2H), 1.97 (m, CH_2CH_2Br and CH_2CH_2O, 4H), 2.69 (t, CH_2COO, 2H), 4.0 (s, CH_3−N, 3H), 4.24 (m, CH_2O and CH_2-N^+, 12H), 6.98 (d, Im−H, 1H), 7.07 (d, Im−H, 1H), 7.7−8.1 (m, Ar−H, 6H), 10.75 (s, Im−H, 1H). MS: 923.4 (this mass was consistent with the fragment without Br^- anion).

Triphenylene imidazolium salts **2a** and **2b** were prepared similarly as above. Since all triphenylene imidazolium salts tended to absorb onto the SEC column, the purity of **2a**−**c** was checked only by TLC. **2a** was obtained as a brown solid with a yield of 70%. ^{1}H NMR (δ, $CDCl_3$): 0.98 (t, CH_3, 15H) 1.44−1.56 (m, $CH_3CH_2CH_2$, 20H), 1.62−1.97 (m, CH_2CH_2O, CH_2CH_2COO, CH_2CH_2Br, 14H), 2.74 (t, CH_2COO, 2H), 3.79 (s, CH_3−N, 3H), 4.24 (m, CH_2O, 10H), 4.48 (s, CH_2-N^+,2H), 7.03−7.13 (m, Im−H, 2H), 7.7−8.1 (m, Ar−H, 6H), 11.27 (s, Im−H, 1H). MS: 839.4 (this mass was consistent with the fragment without Br^- anion). **2b** was obtained as a brown waxlike solid with a yield of 56%. ^{1}H NMR (δ, $CDCl_3$): 0.99 (t, CH_3, 15H) 1.34−1.59 [m, $CH_3CH_2CH_2$ and $(CH_2)_3CH_2CH_2Br$, 26H], 1.87 (m, CH_2CH_2COO, 2H), 1.96 (m, CH_2CH_2Br and CH_2CH_2O, 4H), 2.69 (t, CH_2COO, 2H), 3.76 (s, CH_3−N, 3H), 4.24 (m, CH_2O, 10H), 4.44 (s, CH_2-N^+,2H), 7.10−7.18 (m, Im−H, 2H), 7.7−8.1 (m, Ar−H, 6H), 10.96 (s, Im−H, 1H). MS: 881.4 (this mass was consistent with the fragment without Br^- anion).

Preparation of DNA−Triphenylene Imidazolium Salt Complexes. A small amount of triphenylene imidazolium salts (~20 mg) in THF was added slowly into double-distilled H_2O followed by 5 min sonication in a 100 W ultrasonication bath. A uniform solution with slight turbidity was obtained, and no precipitation was observed. A saturated aqueous solution of purified DNA in the Na form was added dropwise into the aqueous triphenylene imidazolium salt solution. Immediately, DNA−triphynylene imidazolium salt complexes were precipitated out from the aqueous solution. After three times of repeated centrifugation and washing by H_2O to remove free DNA, the DNA−triphenylene imidazolium salt complexes were dried in a vacuum oven at 50 °C for 24 h. To eliminate the possible contamination from extra triphenylene imidazolium salts, the complexes were dissolved in $CHCl_3$ and precipitated in hexane twice. Finally, the complexes were dried in a vacuum oven at 50 °C for 2 days and stored in a refrigerator.

Preparation of Total RNA−Triphenylene Imidazolium Salt Complexes. The preparation procedure for total RNA−triphenylene imidazolium salt complexes was similar to that for the DNA−triphenylene imidazolium salt complexes. However, instead of precipitating out from the aqueous solution, the RNA−triphenylene imidazolium salt complexes formed a hydrogel. Without further purification, the hydrogel was directly dried in a vacuum oven at room temperature for 2 days.

Characterization Methods. Fourier transform infrared (FTIR) spectroscopy was performed on a Necolet 560 spectrometer.

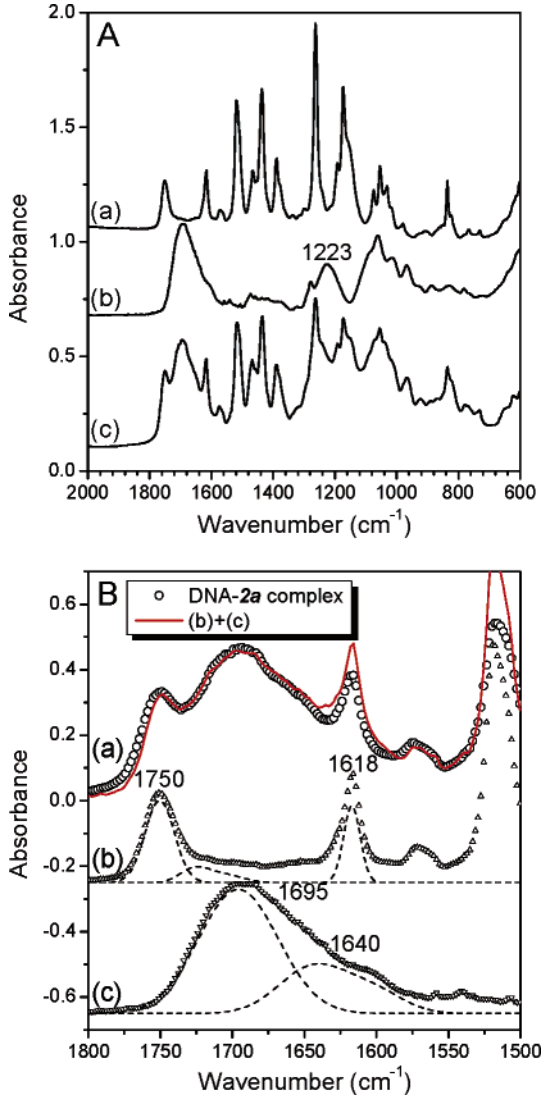

Figure 1. (A) FTIR spectra of (a) **2a**, (b) DNA, and (c) DNA−**2a** complex in the range of 600−2000 cm^{-1}. (B) FTIR spectra in the range of 1500−1800 cm^{-1} for (a) DNA−**2a** complex, (b) **2a**, and (c) DNA. Open symbols represent experimental data. The red solid line is the summation spectrum of (b) and (c). Spectra b and c are deconvoluted into individual absorption bands, shown as the dashed lines, using Peakfit software. Curves are offset for clarity.

Circular dichroism (CD) experiments on thin films (thickness ~ 5 μm) of DNA and DNA−triphenylene imidazolium salt complexes were carried out on a JASCO model 710 spectropolarimeter. Differential scanning calorimetry (DSC) was carried out on a TA Q-100 DSC instrument. Indium standard was used to calibrate the instrument. An ~3 mg sample was used for the DSC study, and the scanning rate was 5 °C/min. 2D XRD was performed using an X-ray tube generator operating at 1.6 kW with a Cr Kα radiation (wavelength λ = 0.229 nm). X-ray data were recorded using a Bruker AXS area detector with a general area detector diffraction system (GADDS). The *d*-spacing was calibrated using silver behenate with the first-order reflection at the scattering vector q = 1.076 nm^{-1}, where $q = (4\pi\sin\theta)/\lambda$ (θ is half scattering angle). Polarized light microscopy (PLM) experiments were performed using an Olympus BX51P microscope equipped with an Instec HCS410 hot-stage. TEM experiments were performed on a Philips EM300 at an accelerating voltage of 80 kV. Thin sections with a thickness of ca. 70 nm were obtained using a Leica Ultracut UCT microtome equipped with a diamond knife at −10 °C. The thin sections were collected onto 400 mesh TEM grids, freeze-dried, and stained by soaking in a 1% uranyl acetate solution for 4 h.[40]

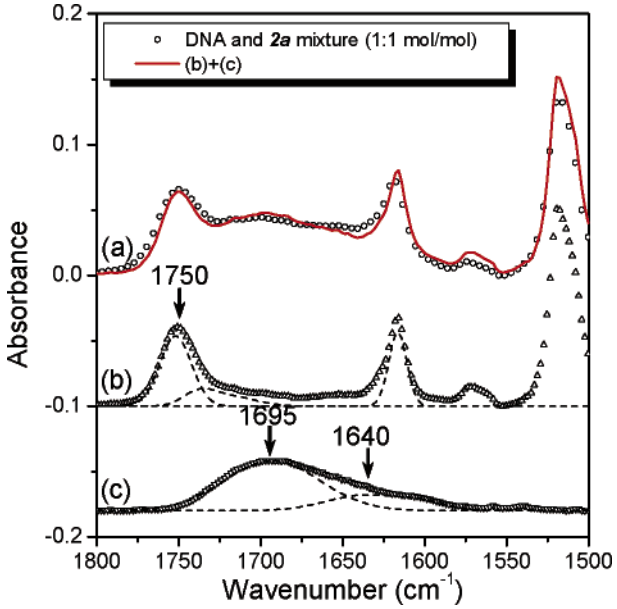

Figure 2. FTIR determination of the carbonyl (C═O) absorptivity ratio of DNA to **2a**. (a) 1:1 mol/mol DNA−**2a** mixture. The open symbols represent experimental data. The red solid line is the summation spectrum of (b) **2a** and (c) DNA. Spectra b and c are deconvoluted into individual absorption bands, shown as the dashed lines, using Peakfit software. Curves are offset for clarity.

Results and Discussion

Determination of Overall Molecular Composition in DNA−Triphenylene Imidazolium Salt Complexes. The overall molecular composition in DNA−triphenylene imidazolium salts was studied by FTIR spectroscopy. Figure 1A shows the FTIR spectra of **2a**, DNA, and DNA−**2a** complex in the range of 600−2000 cm^{-1}. The spectrum of the DNA−**2a** complex possessed both characteristic absorption bands from **2a** and DNA, suggesting the existence of both **2a** and double-strand DNA in the complex. Judging from the absorption band at 1223 cm^{-1} (antisymmetric stretching vibration, $\tilde{\nu}_a\ PO_2^-$) in the DNA FTIR spectrum, DNA adopted the B-form conformation.[52] Figure 1B shows the spectra in the range of 1500−1800 cm^{-1} for the DNA−**2a** complex, **2a**, and DNA. In the spectrum in Figure 1B-b, the absorption band at 1750 cm^{-1} was attributed to the non-hydrogen-bonded ester C═O stretching vibration in **2a** (see Scheme 1). The absorption bands at 1618 and 1516 cm^{-1} were observed due to the stretching motions of C═C in aromatic triphenylene rings.[53] In the DNA spectrum in Figure 1B-c, the peak absorption band at 1695 cm^{-1} was attributed to the hydrogen-bonded C═O stretching in the base pairs [thymine (T), guanine (G), and cytosine (C)].[22,52] The asymmetric shape (a tail in the low wavenumber side) in this absorption band was due to the C═N and C═C stretching in the aromatic bases of DNA around 1640 cm^{-1}.[52] The solid line in Figure 1B-a was a linear addition spectrum from those of **2a** (Figure 1B-b) and DNA (Figure 1B-c). Comparing the addition spectrum (solid line) with the experimental spectrum of the DNA−**2a** complex (open circles) in Figure 1B-a, the two spectra fitted reasonably well.

To determine the molecular composition of the DNA−**2a** complex, the infrared molar absorptivity ratio between the C═O groups in DNA and the C═O groups in **2a** was desired. An FTIR spectrum of the 1:1 (mol/mol) mixture of DNA and **2a** is shown in Figure 2a (open circles). The solid-line spectrum in Figure 2a was a linear addition spectrum from those of **2a** (Figure 2b) and DNA (Figure 2c). Again, this addition spectrum fitted well with the experimental spectrum of the 1:1 DNA and

Table 1. Characterization Data of DNA−2a, DNA−2b, and DNA−2c Complexes

	negative-to-positive charge ratio	T_g (°C)	unit cell density based on X-ray results (g/cm^3)	density (g/cm^3)
DNA−**2a**	1.8/1	8	1.583	1.185
DNA−**2b**	2.0/1	37	1.600[a]	1.150
DNA−**2c**	1.4/1	36	1.200[a]	1.115

[a] The density was calculated by assuming an oblique unit cell with the (10) reflection assigned for the diffuse vertical streaks in the SAXS patterns (Figure 5B,C).

2a mixture. Utilizing Peakfit 4.0 software, individual absorption bands at 1750 cm^{-1} for the non-hydrogen-bonded C═O groups in **2a** and 1695 cm^{-1} for the C═O groups in DNA were deconvoluted, which are shown as the dashed lines in Figure 2b,c. The C═O molar absorptivity ratio between DNA and **2a** was thus calculated to be 2.2, using the peak area ratio between DNA and **2a**. On the basis of this carbonyl molar absorptivity ratio between DNA and **2a**, the molar complexation ratio between the C═O groups in DNA and the C═O groups in **2a** in the DNA−**2a** complex could be estimated around 1.8, using the peak areas at 1695 cm^{-1} in Figure 1B-c and 1750 cm^{-1} in Figure 1B-b. Since [adenine (A)] = [T] and [G] = [C], and each nucleotide has one phosphate group, the molar ratio of the phosphate groups to the C═O groups is 1 in DNA.[54] As a result, the negative-to-positive charge ratio in the DNA−**2a** complex was 1.8.

The FTIR spectra of the DNA−**2b** and DNA−**2c** complexes are shown in Figure 3A,B. The solid-line spectra, again, were the addition spectra of those of DNA and corresponding triphenylene imidazolium salts. Apparently, the addition spectra fitted reasonably well with the experimental spectra of the complexes in open symbols. After peak deconvolution, the molecular compositions (or the negative-to-positive charge ratio) for DNA−**2b** and DNA−**2c** complexes were determined: DNA−**2b** ≈ 2.0 and DNA−**2c** ≈ 1.4. These negative-to-positive charge ratios are summarized in Table 1. It seemed that increasing the spacer length in the triphenylene imidazolium salts from C_5 and C_8 to C_{11}, the negative-to-positive ratio slightly decreased from around 1.8−2.0 to 1.4.

Liquid Crystalline Morphology in DNA−Triphenylene Imidazolium Salt Complexes. The liquid crystalline morphology in the DNA−triphenylene imidazolium salt complexes was first studied by PLM experiments. The PLM micrographs are shown in Figure 4A−C for the DNA−**2a** complex at 150 °C, the DNA−**2b** complex at 135 °C, and the DNA−**2c** complex at 156 °C, respectively. Smectic-like (focal conic) liquid crystalline texture was seen in these micrographs, although the monodomains were small (∼5−15 μm).

Thermal transitions in the DNA−triphenylene imidazolium salt complexes were studied by DSC. The glass transition temperatures (T_g) were observed at 8 °C for the DNA−**2a**, 37 °C for the DNA−**2b**, and 36 °C for the DNA−**2c** (see Table 1). After the first heating to 150 °C at 10 °C/min, liquid crystalline phases developed, as evidenced by the PLM observation of birefringent morphology shown in Figure 4. During the subsequent cooling and heating runs between −60 and 150 °C, no obvious liquid crystalline transitions were observed above the T_g of the DNA−triphenylene imidazolium salt complexes. Also from the PLM experiments, the clearing points for the complexes were above the degradation temperature at 190−200 °C.

The liquid crystalline microstructure of these complexes was investigated by 2D XRD experiments on shear-oriented samples,

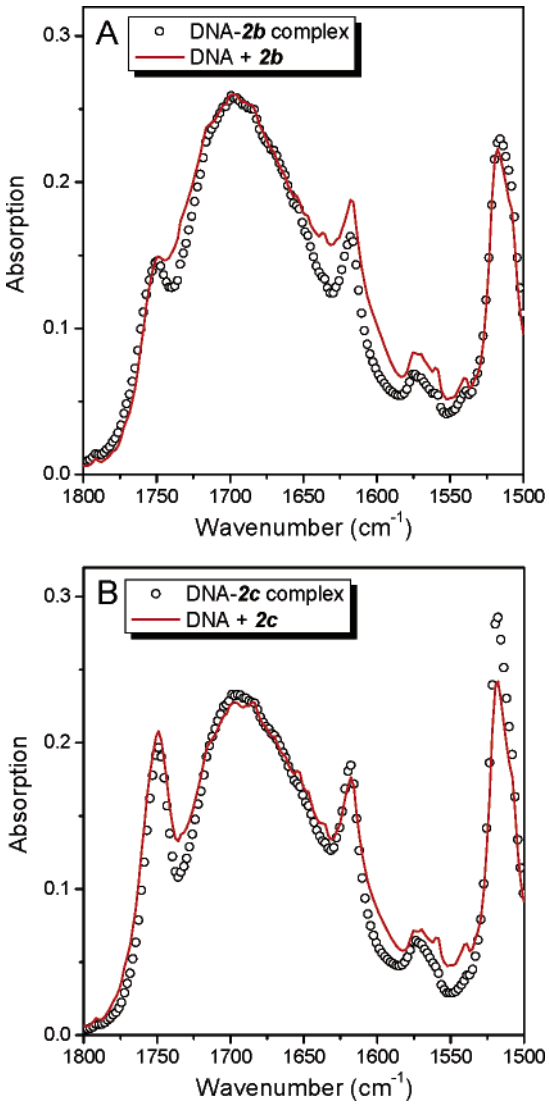

Figure 3. FTIR spectra of (A) DNA−**2b** and (B) DNA−**2c** complexes. The solid lines represent the summation spectra of the DNA and **2b** (or **2c**) spectra.

as shown in Figure 5. The shear experiments were carried out on a hot stage at 150−160 °C by sandwiching the samples between two glass slides. The X-ray beam was directed parallel to the shear plane. The SAXS pattern in Figure 5A shows the columnar liquid crystalline structure of the DNA−**2a** complex, while the wide-angle X-ray diffraction (WAXD) pattern in Figure 5D shows the molecular level packing. Lamellar reflections with a q-ratio being 1:2:3 were seen on the meridian of Figure 5A with two sets of reflections, (10) and (11), in the quadrant. Note that even-order layer reflections on the meridian appeared weaker than the odd-order reflections, which was attributed to the form factor effect when the thicknesses of DNA and triphenylene layers were similar. No reflections were observed on the equator. This SAXS pattern, with the indices shown in Figure 5A, could be explained by an oblique 2D structure demonstrated in Figure 6A. The unit cell dimensions were thus obtained as a = 1.73 nm, b = 4.55 nm, and α = 111°. In the corresponding WAXD pattern in Figure 5D, beyond the amorphous halo, a pair of reflections were seen on the equator with a d-spacing of 0.355 nm, suggesting the face-to-face distance between neighboring triphenylene molecules formed through $\pi-\pi$ stacking.[55] As we know, DNA double helices had a diameter of ∼2.0 nm, and the triphenylene molecules with C_5 side chains had an intercolumnar distance

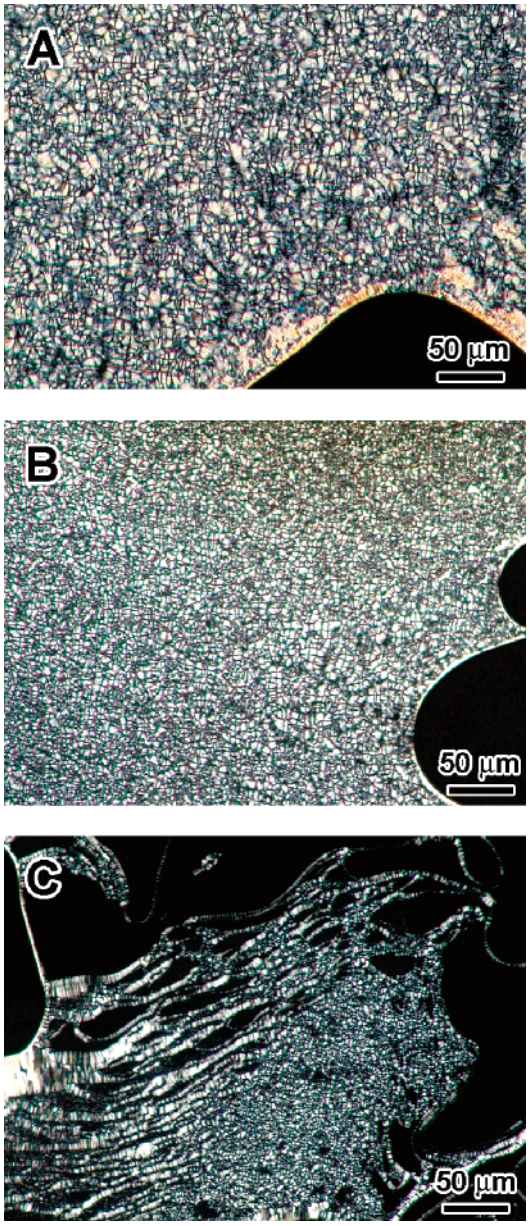

Figure 4. PLM micrographs for (A) DNA−**2a** at 150 °C, (B) DNA−**2b** at 135 °C, and (C) DNA−**2c** at 156 °C.

of ∼1.7 nm.[55] Judging from the overall layer thickness of 4.55 nm, it was reasonable to assume double-layered triphenylene columns and a single-layered DNA with a relatively tight lateral packing, as shown in Figure 6A. In this structure, one pair of phosphates at each side of a DNA repeat was complexed to two triphenylene imidazolium salt molecules.

2D SAXS and WAXD patterns for the shear-oriented DNA−**2b** complex are shown in Figure 5B,E. The lamellar reflections (*d*-spacing of 5.32 nm) were still observed on the meridian with up to four orders of reflections. Again, the even-order reflections appeared weaker than the odd-order ones. The larger layer spacing was consistent with the increase in the spacer length from C_5 to C_8. A drastic change in the SAXS pattern from that in Figure 5A was the fact that the quadrant reflections became four diffuse streaks. Since these striations oriented perpendicular to the shear (or the lamellar) plane, they indicated a loss of positional correlation among adjacent layers for both triphenylene columns and DNA double strands. The formation of vertical striation was also reported in the high-temperature L_α^C phase for DNA lipoplexes.[21] However, the maximum intensity of these vertical striations in the quadrant instead of on the equator suggested that the oblique arrangement of triphenylene columns and DNA double strands preserved to a certain degree in each layer. The vertical rodlike shape of these striations also indicated that the in-plane correlation length was much longer than the out-of-plane correlation length. This SAXS pattern was assigned as a double lamello-columnar (Col_L) structure with both triphenylene and DNA forming columns (Figure 6B). The diffuse, vertically oriented streaks suggested that there was only a short-range order among the double-layered triphenylene and DNA columns. The interdisk spacing in the columns (0.349 nm) was obtained from oriented reflections on the equator in Figure 5E.

For shear-oriented DNA−**2c** complex, the 2D SAXS and WAXD patterns are shown in Figure 5C,F. The SAXS pattern in Figure 5C was very similar to that in Figure 5B, except that the lamellar *d*-spacing increased to 5.98 nm as the spacer length increased to C_{11}, suggesting again a Col_L phase in the DNA−**2c** complex. The face-to-face interdisk spacing of 0.342 nm was evidenced by a pair of reflections on the equator, as shown in Figure 5F. From the above observations, a transition from Col_o to Col_L occurred by simply increasing the spacer lengths from C_5 to C_8 and C_{11}.

The lamellar morphology in DNA−triphenylene imidazolium salt complexes was also studied by TEM. Lamellar morphology for the DNA−**2a** complex is clearly seen in Figure 7A and its inset. Since DNA was preferentially stained by uranyl acetate, DNA layers appeared dark in the micrograph. As one can see, a long-range order of the lamellar packing over a couple hundred nanometers existed, and this was much higher than those reported for DNA lipoplex colloidal particles.[23,24,30,42,43] Figure 7B and its inset show a lamellar structure in the DNA−**2c** complex. From both TEM micrographs, both overall layer spacing was comparable to the SAXS results.

In a double-strand DNA, the distance separating adjacent planes of hydrogen-bonded base pairs was 0.34 nm, close to the $\pi-\pi$ stacking distance of 0.34−0.35 nm in the triphenylene columns.[31] Therefore, the XRD results suggested that the complexation ratio between the phosphate groups in DNA and the imidazolium salts should be 1:1, lower than the values of 1.4−2.0 determined by FTIR experiments (see Table 1). Taking into account of two triphenylene imidazolium salts per DNA base-pair in a unit cell (Figure 6), the density of the pure DNA−**2a** complex was calculated to be 1.583 g/cm^3. The experimental density of the DNA−**2a** complex, 1.185 g/cm^3 (see Table 1), was lower than the calculated value based on the X-ray results. This was the same for the DNA−**2b** and DNA−**2c** complexes, as shown in Table 1. Both lower density and higher negative-to-positive charge ratio in the experimental results suggested that only parts of a DNA chain were complexed with triphenylene imidazolium salts, which was consistent with other reports for the DNA−dendritic cationic polymer complexes[45,46] and DNA−histone complexes.[9] It was speculated that the complex formation (or precipitation) from the aqueous solution was too fast to allow complete complexation between DNA and the triphenylene imidazolium salt molecules.

Double-Strand DNA Conformation in DNA−Triphenylene Imidazolium Salt Complexes. As mentioned previously in Figure 1, DNA adopted the B-form conformation in the solid state. This is further evidenced by the CD spectrum in Figure 8, where the Cotton effect has a positive peak around 276 nm. However, this Cotton effect completely disappeared for thin films of DNA−triphenylene imidazolium salt complexes, suggesting a severe disturbance in the DNA helical conformation.

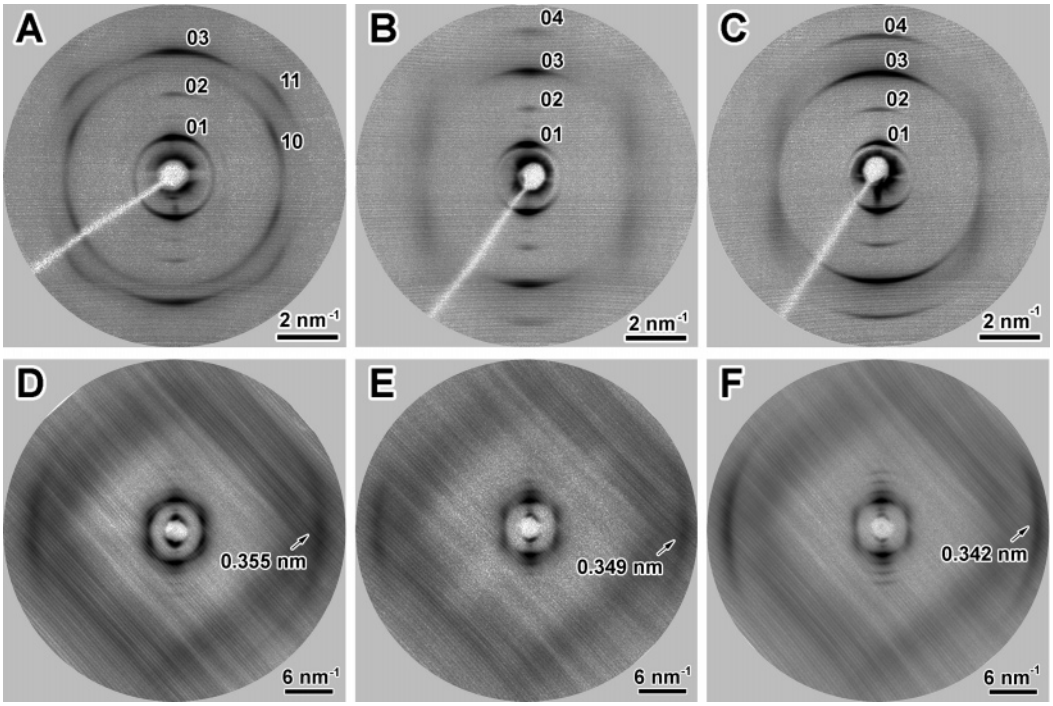

Figure 5. 2D X-ray diffraction patterns for shear-oriented DNA−**2a** [(A) SAXS and (D) WAXD], DNA−**2b** [(B) SAXS and (E) WAXD], and DNA−**2c** [(C) SAXS and (F) WAXD] complexes. Note that the off-equator vertical striations in (B) and (C) suggest a loss of positional correlation among adjacent layers for obliquely arranged triphenylene columns and DNA double strands.

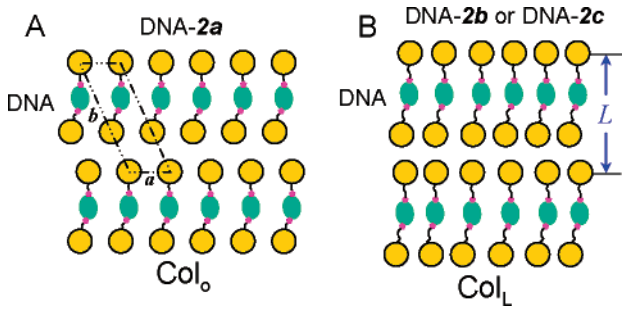

Figure 6. Schematic representations of (A) an oblique-columnar phase for the DNA−**2a** complex and (B) a lamello-columnar phase for the DNA−**2b** and DNA−**2c** complexes.

This could be understood from the molecular packing as shown in Figure 6. In the complexed parts of DNA, the negative phosphate to positive imidazolium salt ratio was 1:1, and two triphenylene columns were attached to the opposite sides of a double-strand DNA repeat. It was the formation of the triphenylene columns that destroyed or unwound the helical conformation of double-strand DNA conformation. Although there were uncomplexed DNA moieties, their conformation might also be disturbed, to a great extent, by the strong ionic interactions in the system.

Comparison with Single-Strand Total RNA−Triphenylene Imidazolium Salt Complexes. Before comparing to RNA−triphenylene imidazolium salt complexes, the morphology of pure triphenylene imidazolium salts was studied. As an example, the structural comparison between **2a** and its complex with DNA is shown in Figure 9. Before isotropization **2a** showed only a crystalline phase. From a DSC study, its melting point (single peak) was 71 °C with a heat of transition being 21.5 kJ/mol, which suggested a single crystalline structure in the sample. The crystalline morphology is further confirmed by SAXS and WAXD profiles in Figure 9. Apparently, the SAXS and WAXD profiles are drastically different from those of the liquid crystalline DNA−**2a** complex in Figure 9. The inset of Figure

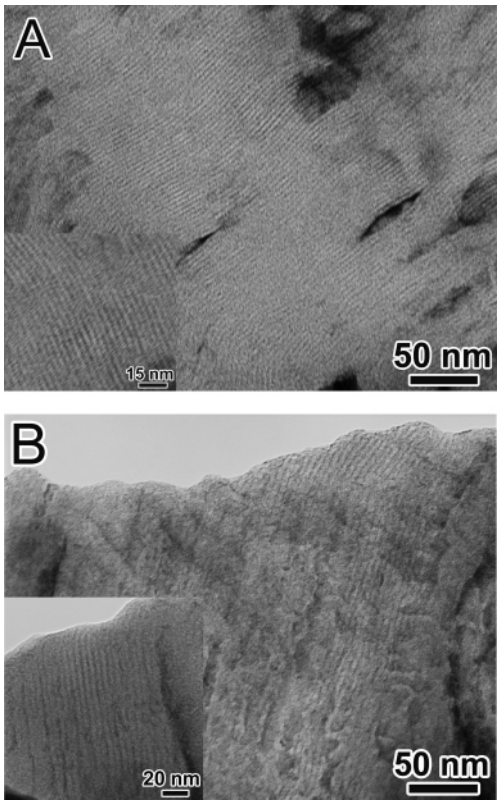

Figure 7. Bright-field TEM micrographs of (A) DNA−**2a** and (B) DNA−**2c**. The thin sections were stained by immersing in a 1 wt % uranyl acetate aqueous solution for 4 h.

9B also shows a PLM micrograph for **2a** with typical spherulitic crystalline morphology. The crystal structures of hexakis(alkyloxy)triphenylenes with six $-OC_nH_{2n+1}$ ($n = 1-5$) side chains have been determined from single-crystal X-ray crystallography.[56,57] For hexakis(pentyloxy)triphenylene, the crystalline structure was determined to be a hexagonal structure with $a =$

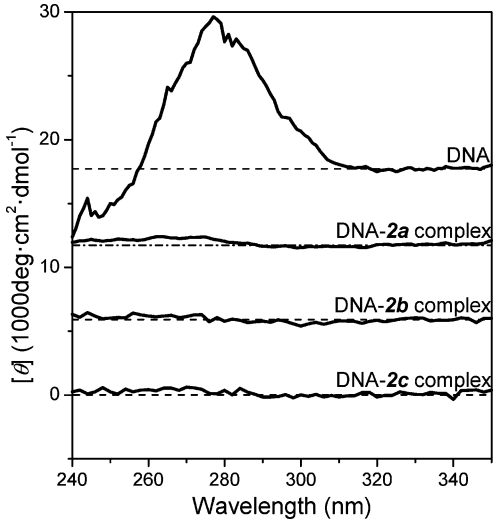

Figure 8. Thin film CD spectra of DNA, DNA−**2a**, DNA−**2b**, and DNA−**2c** complexes. Curves are offset for clarity.

2.03 nm and $c = 0.352$ nm.[57] However, the first reflection for **2a** showed a *d*-spacing of 3.63 nm, much larger than the *a*-axis of 2.03 nm. The crystalline structure therefore must be different from that of hexakis(pentyloxy)triphenylene. The detailed crystalline structure of **2a** needs future investigations but will not be elaborated here. As we can see, the liquid crystalline structure of the triphenylene imidazolium salt was different from their ionic complexes with DNA.

To understand the effect of chain rigidity of double-strand DNA on the supramolecular complexation with triphenylene imidazolium salts, single-strand total RNA was used to blend with triphenylene imidazolium salts. An example of the RNA and **2a** blends at different charge ratios is shown in Figure 10. An apparent difference between RNA and DNA for their complexes with **2a** was that RNA−**2a** complexes did not precipitate out from the aqueous solution upon immediate mixing in the aqueous solution. Instead, they formed a gel, as shown in the inset of Figure 10A for the RNA−**2a** blend with a negative-to-positive ratio (N_{RNA}/P_{2a}) of 4:1. Also, the hydrogel formation made it difficult to eliminate possible contaminations from free RNA and **2a**. Therefore, all RNA−**2a** blends were dried directly before characterization. For RNA−**2a** blends with $N_{RNA}/P_{2a} = 1:1$ and 2:1, lamellar morphology was observed with *d*-spacings being 5.3 and 5.6 nm, respectively. The second-order reflections were not clear, and the third reflections overlapped with a broad peak. However, for RNA−**2a** with $N_{RNA}/P_{2a} = 4:1$, the lamellar structure, having a *q*-ratio of 1:2:3 in Figure 10B, had a much smaller *d*-spacing of 2.1 nm. Note that the average spacing between neighboring triphenylene in a columnar liquid crystalline phase was 1.7 nm. It was reasonable to infer that for RNA−**2a** with $N_{RNA}/P_{2a} = 1:1$ and 2:1 double-layer discotic triphenylene (3.4 nm) alternated with the RNA layer (∼2 nm), while for RNA−**2a** with $N_{RNA}/P_{2a} = 4:1$, an interdigitated discotic morphology was obtained. This was understandable because only when the amount of **2a** decreased, the interdigitation of the triphenylene disks occurred.

However, it was still not clear how the triphenylene discotic molecules self-assembled in the RNA−**2a** complexes. First, there was no face-to-face interdisk reflection around 17.6 nm^{-1} (*d*-spacing of 0.35−0.36 nm) for the RNA−**2a** complexes at all compositions, as opposed to the DNA−**2a** complex WAXD results in Figure 9B. Second, the broad peaks around 3.5 nm^{-1} for the RNA−**2a** complexes with $N_{RNA}/P_{2a} = 1:1$ and 2:1 could be an overlap of the third-order reflection from the lamellar structure and the nematic-type of packing in the discotic triphenylenes. The discotic nematic-type packing of the triphenylene disks was proved by 2D WAXD pattern of a shear-oriented RNA−**2a** sample in Figure 11. Lamellar reflections were seen on the meridian with a *q*-ratio being 1:3:4:6, while a broad discotic nematic scattering ring was seen as indicated by the arrow in Figure 11. On the basis of the above analysis, a schematic of the RNA−triphenylene imidazolium salt complexes is illustrated in Figure 12. Obviously, no columnar liquid crystalline morphology was observed in single-strand RNA−**2a** complexes, which was contrary to the double-strand DNA−**2a** complexes. We speculate that the higher chain rigidity of the double-strand DNA than total RNA may be responsible for the formation of ordered columnar liquid crystalline self-assembly.

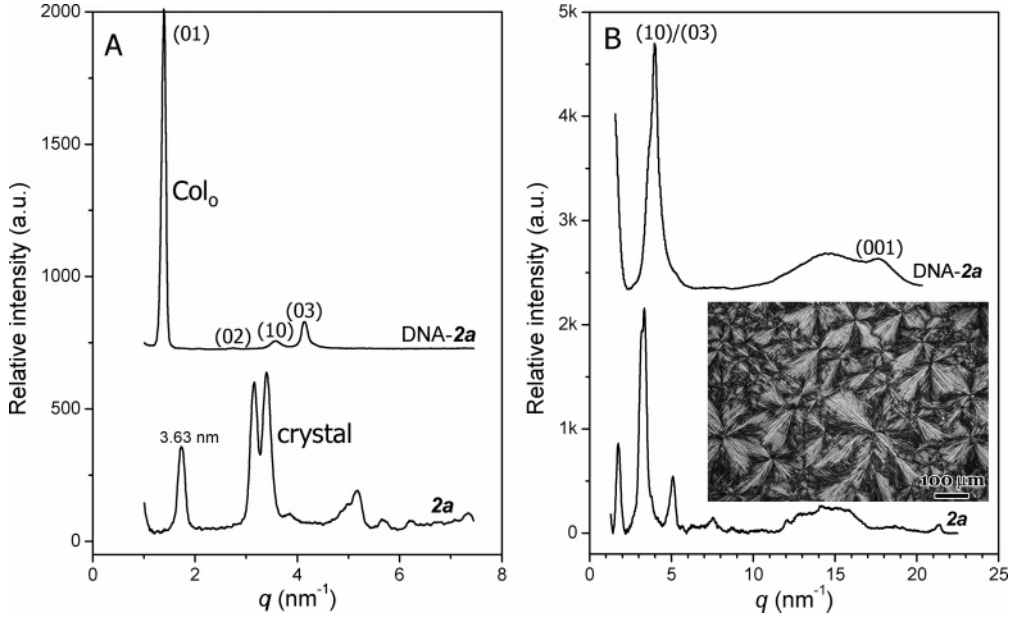

Figure 9. (A) SAXS and (B) WAXD profiles for DNA−**2a** complex and **2a** at room temperature. The inset in (B) is a PLM micrograph of **2a** spherulites at 66 °C.

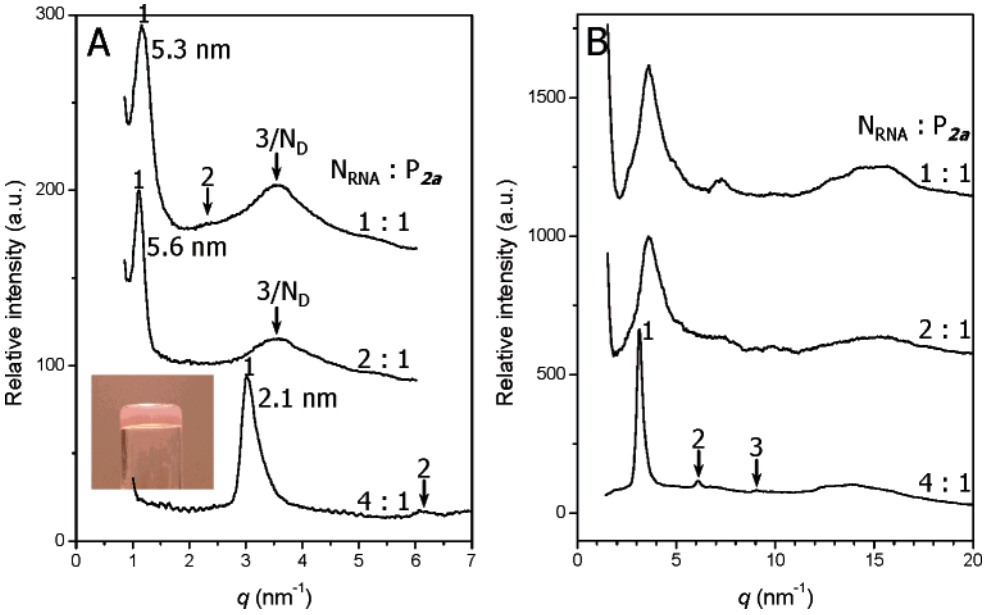

Figure 10. (A) SAXS and (B) WAXD profiles for RNA−**2a** blends with negative-to-positive (N_{RNA}/P_{2a}) ratios being 1:1, 2:1, and 4:1. The inset in (A) is a picture of a RNA−**2a** (4:1) hydrogel.

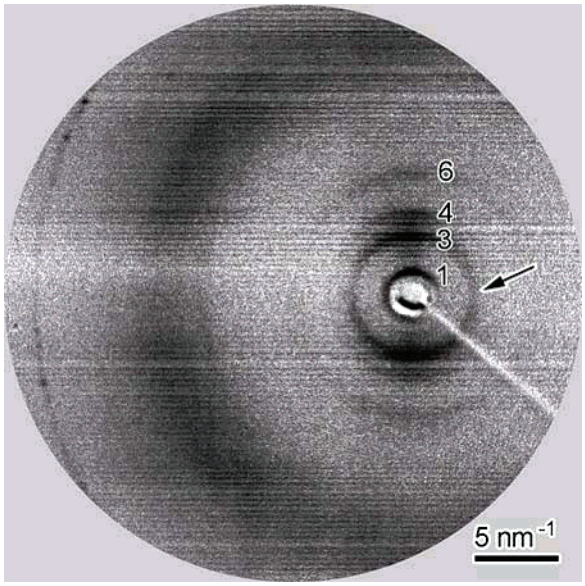

Figure 11. 2D WAXD pattern for the RNA−**2a** complex with N_{RNA}/P_{2a} = 1:1. Layer reflections are labeled with numbers, and the arrow indicates the scattering from the discotic nematic-type packing from the triphenylene molecules.

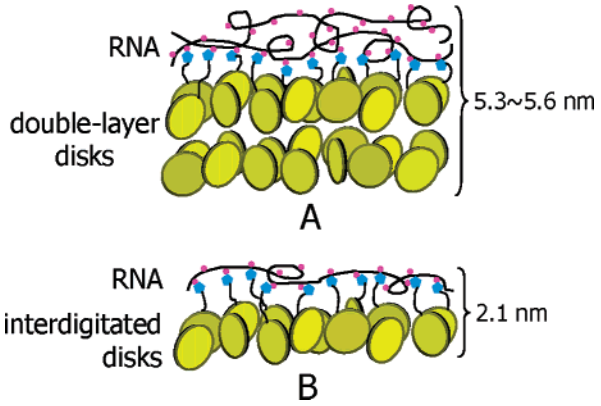

Figure 12. Schematic representations of (A) double-layer RNA−**2a** with N_{RNA}/P_{2a} = 1:1 and 2:1 and (B) single-layer interdigitated RNA−**2a** with N_{RNA}/P_{2a} = 4:1. The dots represent phosphate anions, and the pentagons represent imidazolium cations. The triphenylene disks are represented by yellow circles.

Conclusions

In conclusion, we have for the first time studied the supramolecular complexation between DNA and asymmetric triphenylene imidazolium salts with various spacer lengths. The molecular composition of the DNA−triphenylene imidazolium salt complexes was quantitatively determined by FTIR, with the phosphate-to-imidazolium salt ratio ranging from 2.0 to 1.4 for different spacer lengths. 2D XRD experiments were employed to determine the columnar liquid crystalline self-assembly in the complexes. As the spacer length increased from C_5 to C_8 and C_{11}, a morphological transition from Col_o to Col_L was observed. The XRD analysis suggested a 1:1 complexation ratio between the phosphate groups in DNA and triphenylene imidazolium salts. It was therefore inferred that the DNA chains were only partially complexed. The formation of triphenylene columns destroyed DNA helical conformation, as evidenced by the CD study. A comparison was made to total RNA complexation with triphenylene imidazolium salts. Only lamellar morphology with random discotic triphenylene molecules sandwiched between RNA layers was observed. The absence of columnar ordering in the RNA−triphenylene imidazolium salt complexes was attributed to the flexibility of the RNA chains as opposed to double-strand DNA chains. In the future, detailed studies on a larger range of spacer lengths will be performed to understand where the morphological transition exactly occurs.

Acknowledgment. This work was supported by NSF CAREER award DMR-0348724, DuPont Young Professor Grant, and 3M Nontenured Faculty Award.

References and Notes

(1) *Interactions of Surfactants with Polymers and Proteins*; Goddard, E. D., Ananthapadmanabhan, K. P., Eds.; CRC Press: Boca Raton, FL, 1993; Chapters 4 and 5.
(2) *Polymer-Surfactant Systems*; Kwak, J. C. T., Eds.; Marcel Dekker: New York, 1998.
(3) *Physical Chemistry of Polyelectrolytes*; Radeva, T., Ed.; Marcel Dekker: New York, 2001; Part III.

(4) Antonietti, M.; Burger, C.; Thunemann, A. *Trends Polym. Sci.* **1997**, *5*, 262−267.
(5) MacKnight, W. J.; Ponomarenko, E. A.; Tirrell, D. A. *Acc. Chem. Res.* **1998**, *31*, 781−788.
(6) Zhou, S.; Chu, B. *Adv. Mater.* **2000**, *12*, 545−556.
(7) Bloomfield, V. A. *Curr. Opin. Struct. Biol.* **1996**, *6*, 334−341.
(8) Safinya, C. R. *Curr. Opin. Struct. Biol.* **2001**, *11*, 440−448.
(9) Elgin, S. C. R.; Workman, J. L. *Chromatin Structure and Gene Expression*; Oxford University Press: New York, 2000.
(10) Pitard, B. *Somat. Cell Mol. Genet.* **2002**, *27*, 5−15.
(11) Zhdanov, R. I.; Podobed, O. V.; Vlassov, V. V. *Bioelectrochemistry* **2002**, *58*, 53−64.
(12) Bruinsma, R. *Eur. Phys. J. B* **1998**, *4*, 75−88.
(13) Harries, D.; May, S.; Gelbart, W. M.; Ben-Shaul, A. *Biophys. J.* **1998**, *75*, 159−173.
(14) Koltover, I.; Salditt, T.; Safinya, C. R. *Biophys. J.* **1999**, *77*, 915−924.
(15) Widom, J. *Annu. Rev. Biophys. Biomol. Struct.* **1998**, *27*, 285−327.
(16) Daban, J.-R. *Biochem. Cell Biol.* **2003**, *81*, 91−99.
(17) Dincer, S.; Tuerk, M.; Piskin, E. *Gene Ther.* **2005**, *12*, S139−S145.
(18) Schmidt-Wolf, G. D.; Schmidt-Wolf, I. G. H. *Trends Mol. Med.* **2003**, *9*, 67−72.
(19) Felgner, P. L.; Gadek, T. R.; Holm, M.; Roman, R.; Chan, H. W.; Wenz, M.; Northrop, J. P.; Ringold, G.; M.; Danielsen, M. *Proc. Natl. Acad. Sci. U.S.A.* **1987**, *84*, 7413−7417.
(20) Rädler, J. O.; Koltover, I.; Salditt, T.; Safinya, C. R. *Science* **1997**, *275*, 810−814.
(21) Artzner, F.; Zantl, R.; Rapp, G.; Rädler, J. O. *Phys. Rev. Lett.* **1998**, *81*, 5015−5018.
(22) Pohle, W.; Selle, C.; Gauger, D. R.; Zantl, R.; Artzner, F.; Rädler, J. O. *Phys. Chem. Chem. Phys.* **2000**, *2*, 4642−4650.
(23) Lasic, D.; Strey, H.; Stuart, M.; Podgornik, R.; Frederik, P. M. *J. Am. Chem. Soc.* **1997**, *119*, 832−833.
(24) Mel'nikova, Y.; Mel'nikov, S. M.; Löfroth, J. E. *Biophys. Chem.* **1999**, *81*, 125−141.
(25) Barreleiro, P. C. A.; Lindman, B. *J. Phys. Chem. B* **2003**, *107*, 6208−6213.
(26) Koynova, R.; MacDonald, R. C. *Biophys. J.* **2003**, *85*, 2449−2465.
(27) Koynova, R.; MacDonald, R. C. *Nano Lett.* **2004**, *4*, 1475−1479.
(28) MacDonald, R. C.; Ashley, G. W.; Shida, M. M.; Rakhmanova, V. A.; Tarahovsky, Y. S.; Pantazatos, D. P.; Kennedy, M. T.; Pozharski, E. V.; Baker, K. A.; Jones, R. D.; Rosenzweig, H. S.; Choi, K. L.; Qiu, R.; Mcintosh, T. J. *Biophys. J.* **1999**, *77*, 2612−2629.
(29) Kennedy, M. T.; Pozharski, E. V.; Rakhmanova, V. A.; MacDonald, R. C. *Biophys. J.* **2000**, *78*, 1620−1633.
(30) Pitard, B.; Oudrhiri, N.; Vigneron, J.-P.; Hauchecorne, M.; Aguerre, O.; Toury, R.; Airiau, M.; Ramasawmy, R.; Scherman, D.; Crouzet, J.; Lehn, J.-M.; Lehn, P. *Proc. Natl. Acad. Sci. U.S.A.* **1999**, *96*, 2621−2626.
(31) Tanaka, K.; Okahata, Y. *J. Am. Chem. Soc.* **1996**, *118*, 10679−10683.
(32) Nakayama, H.; Ohno, H.; Okahata, Y. *Chem. Commun.* **2001**, 2300−2301.
(33) Lin, A. J.; Slack, N. L.; Ahmad, A.; Koltover, I.; George, C. X.; Samuel, C. E.; Safinya, C. R. *J. Drug Target* **2000**, *8*, 13−27.
(34) O'Hern, C. S.; Lubensky, T. C. *Phys. Rev. Lett.* **1998**, *80*, 4345−4348.
(35) O'Hern, C. S.; Lubensky, T. C. *Phys. Rev. E* **1998**, *58*, 5948−5965.
(36) Golubovic, L.; Golubovic, M. *Phys. Rev. Lett.* **1998**, *80*, 4341−4344.
(37) Golubovic, L.; Lubensky, T. C.; O'Hern, C. S. *Phys. Rev. E* **2000**, *62*, 1069−1094.
(38) Koltover, I.; Salditt, T.; Rädler, J. O.; Safinya, C. R. *Science* **1998**, *281*, 78−81.
(39) Schmutz, M.; Durand, D.; Debin, A.; Palvadeau, Y.; Etienne, A.; Thierry, A. R. *Proc. Natl. Acad. Sci. U.S.A.* **1999**, *96*, 12293−12298.
(40) Gershon, H.; Ghirlando, R.; Guttman, S.; Minsky, A. *Biochemistry* **1993**, *32*, 7143−7151.
(41) Hubner, S.; Battersby, B. J.; Grimm, R.; Cevc, G. *Biophys. J.* **1999**, *76*, 3158−3166.
(42) Pitard, B.; Oudhiri, N.; Vigneron, J. P.; Lambert, O.; Vivien, E.; Hauchecorne, M.; Scherman, D.; Rigaud, J. L.; Lehn, J. M.; Lehn, P. *J. Gene Med.* **2001**, *3*, 478−487.
(43) Battersby, B. J.; Grimm, R.; Huebner, S.; Cevc, G. *Biochim. Biophys. Acta* **1998**, *1372*, 379−383.
(44) Evans, H. M.; Ahmad, A.; Ewert, K.; Pfohl, T.; Martin-Herranz, A.; Bruinsma, R. F.; Safinya, C. R. *Phys. Rev. Lett.* **2003**, *91*, 075501/1-075501/4.
(45) Goessl, I.; Shu, L.; Schlueter, A. D.; Rabe, J. P. *J. Am. Chem. Soc.* **2002**, *124*, 6860−6865.
(46) Gossl, I.; Shu, L.; Schluter, A. D.; Rabe, J. P. *Single Mol.* **2002**, *3*, 315−316.
(47) Chen, G.; Han, X.; Zhang, L.; Ye, J. *J. Chromatogr. A* **2002**, *954*, 267−276. The molar content of G + C bases was determined as 49 mol %.
(48) Crestfield, A. M.; Smith, K. C.; Allen, F. W. *J. Biol. Chem.* **1955**, *216*, 185−193. The A, U, G, and C base compositions were determined for yeast RNA, and its molecular weight depends on enzymatic degradation during the extraction process.
(49) Allen, M. T.; Diele, S.; Harris, K. D. M.; Hegmann, T.; Kariuki, B. M.; Lose, D.; Preece, J. A.; Tschierske, C. *J. Mater. Chem.* **2001**, *11*, 301−311.
(50) Boden, N.; Borner, R. C.; Bushby, R. J.; Cammidge, A. N.; Jesudason, M. V. *Liq. Cryst.* **1993**, *15*, 851−858.
(51) Kumar, S.; Manickam, M. *Synthesis* **1998**, 1119−1122.
(52) Fabian, H.; Bohm, S.; Becker, M. *Stud. Biophys.* **1978**, *72*, 99−106.
(53) Pouchert, C. J. *The Aldrich Library of FT-IR Spectra*, 2nd ed.; Aldrich: Milwaukee, 1997.
(54) Assuming [A] = [T] = x and [G] = [C] = y, the phosphate content will be $2(x + y)$. Since T has two C═O groups, and G and C each contains one C═O group, the carbonyl content is still $2(x + y)$. The ratio between the phosphate and carbonyl groups is thus always 1.
(55) Cui, L.; Miao, J.; Zhu, L.; Sics, I.; Hsiao, B. S. *Macromolecules* **2005**, *38*, 3386−3394.
(56) Andresen, T. L.; Krebs, F. C.; Thorup, N.; Bechgaard, K. *Chem. Mater.* **2000**, *12*, 2428−2433.
(57) Li, G.; Luo, J.; Wang, T.; Zhou, E.; Huang, J.; Bengs, H.; Ringsdorf, H. *Mol. Cryst. Liq. Cryst.* **1998**, *309*, 73−91.

MA060001X